

Article

Adhesion-Increased Carbon Nanowalls for the Electrodes of Energy Storage Systems

Hyeokjoo Choi ¹, Seokhun Kwon ¹, Hyunil Kang ¹, Jung Hyun Kim ² and Wonseok Choi ^{1,*}

¹ Department of Electrical Engineering, Hanbat National University, Daejeon 34158, Korea; hyukju1210@hanmail.net (H.C.); kwon1567@naver.com (S.K.); hikang@hanbat.ac.kr (H.K.)

² Department of Advanced Materials Engineering, Hanbat National University, Daejeon 34158, Korea; jhkim2011@hanbat.ac.kr

* Correspondence: wschoi@hanbat.ac.kr

Received: 8 November 2019; Accepted: 9 December 2019; Published: 13 December 2019



Abstract: Carbon nanowalls (CNWs), which are used as electrodes for secondary batteries in energy storage systems (ESSs), have the widest reaction surface area among the carbon-based nanomaterials, but their application is rare due to their low adhesion with substrates. Indium tin oxide (ITO), a representative transparent conducting oxide (TCO) material, is widely used as the electrode for displays, solar cells, etc. Titanium nitride (TiN) is a well-used material as an interlayer for improving the adhesion between two materials. In this study, ITO or TiN thin films were used as an interlayer to improve the adhesion between a CNW and a substrate. The interlayer was deposited on the substrate using a radio frequency (RF) magnetron sputtering system with a four-inch TiN or ITO target. CNWs were grown on the interlayer-coated substrate using a microwave-plasma-enhanced chemical vapor deposition (MPECVD) system with a mixture of methane (CH₄) and hydrogen (H₂) gases. The adhesion of the CNW/interlayer/substrate structure was observed through ultrasonic cleaning.

Keywords: carbon nanomaterials; carbon nanowall; adhesion; energy storage system

1. Introduction

Many studies on energy storage systems (ESSs) are under way for the development of renewable energy for buildings [1–3]. Among ESSs, the battery is the main element, and carbon is often used as the secondary electrode of the battery [4,5]. Carbon nanowalls (CNWs) are wall-shaped graphite nanomaterials with graphene sheets standing vertically in a lamellar structure and connected to one another [6–8]. Therefore, three-dimensional graphene sheets have the largest reaction area among all the graphite nanomaterials. In addition, while graphene [9] and carbon nanotubes (CNTs) [10] need catalysts to grow, CNWs can grow directly on a substrate, without catalysts, making them relatively cheaper to grow than graphene and CNTs, which is a huge advantage from an engineering standpoint. In addition, CNWs can be grown through various chemical vapor deposition (CVD) methods with effectual field emission characteristics [11–15].

The disadvantage of CNWs, however, is their low adhesion to the substrate. The walls easily break down under very small stresses, and the substrate and CNW can be separated from each other. Low-adhesion materials, of course, have limited application. Among the photolithography processes commonly used as a semiconductor process [16,17], the lift-off process is a process of removing a photoresist (PR) layer, in which a sample is submerged in acetone and ultrasonic cleaning is performed for a predetermined time to leave only the desired material. A CNW grown directly on a substrate dissociates from the acetone, like the PR layer, when the lift-off process is performed. Therefore, the desired sample cannot be obtained and cannot be used in the desired application.

In this study, an intermediate layer (interlayer) was inserted between the CNW and the substrate to increase the adhesion of the former to the latter. Indium tin oxide (ITO) and titanium nitride (TiN) were used as the intermediate layer. ITO is a typical transparent conducting oxide (TCO) and is intensively studied for displays and liquid crystal panels [18–20], among others, while TiN is a typical interlayer [21,22] with excellent thermal stability and chemical safety, and with high fine hardness. These two widely used materials were deposited to a thickness of about 150 nm using a four-inch ITO or TiN target, with a radio frequency (RF) magnetron sputtering system. The CNW was grown by injecting a mixture of hydrogen (H_2) and methane (CH_4) gases into the interlayer deposited in a microwave-plasma-enhanced chemical vapor deposition (MPECVD) chamber. After the sample was submerged in acetone, its surface properties before and after ultrasonic cleaning were confirmed via field emission scanning electron microscopy (FESEM), and the chemical compositions of the dissociated and undissolved parts were examined via energy-dispersive X-ray spectroscopy (EDS). The Raman spectra were used to observe the structural characteristics of the CNW grown on the interlayer and of the CNW grown directly on the substrate. X-ray photoelectron spectrometry (XPS) confirmed the chemical bonding of the CNW grown on the interlayer. The electrical properties of the CNW grown directly on the substrate were compared with those of the CNW grown on the interlayer before and after ultrasonic cleaning, using Hall measurement.

2. Experiment

2.1. Interlayer Deposition

The prepared $2 \times 2 \text{ cm}^2$ p-type silicon (Si) wafers (100) were cleaned with trichlorethylene (TCE), acetone, methanol, and deionized water to remove any foreign substances, and then they were ultrasonically cleaned for 10 min, in that order [23]. The washed Si wafers were then dried with nitrogen (N_2) gas. The cleaned Si wafers were then placed in a radio frequency (RF) magnetron sputtering system (Figure 1a) chamber, and the base vacuum was kept at below 10^{-5} Torr. Four-inch TiN and ITO targets were used. The ITO target was sputtered for 10 min at 100 W RF power and 1.0×10^{-2} Torr working vacuum while the TiN target was sputtered for 45 min at 150 W RF power and 1.5×10^{-2} Torr working vacuum. Then, 40 sccm argon gas was added to both at room temperature, and each was attached to a substrate via spinning at 1700 rpm during deposition.

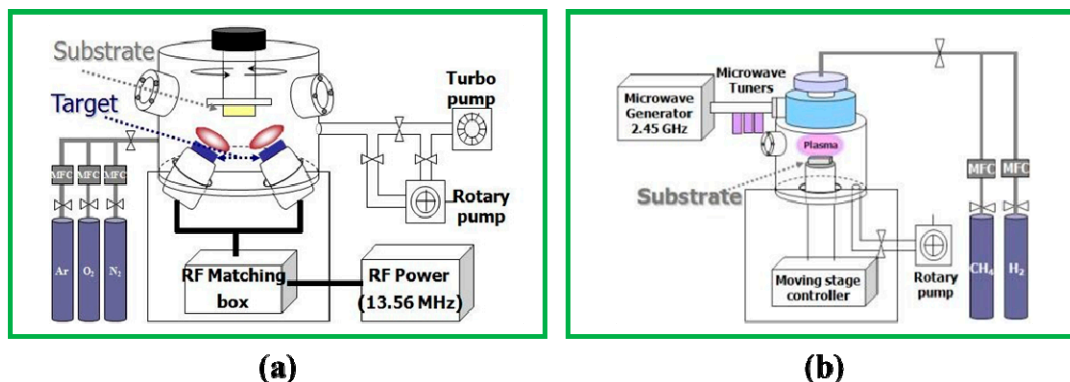


Figure 1. Schematic of the (a) RF magnetron sputtering system and (b) MPECVD.

2.2. Carbon Nanowall Growth

After a $5 \times 5 \text{ mm}^2$ mask was placed on the ITO- and TiN-deposited Si wafers in the MPECVD chamber (ASTeX-type MPECVD, Woosin CryoVac, 2.45 GHz microwave) in Figure 1b, the base vacuum was maintained at 10^{-4} Torr. A mixture of H_2 gas (25 sccm) and CH_4 gas (55 sccm), to be used as a plasma ball above the substrate, was added to grow a CNW on the interlayer-coated substrate for 10 min. At a $700 \text{ }^\circ\text{C}$ holder temperature, the working vacuum was fixed at 5.5×10^{-2} Torr, and the

microwave power was 1300 W through quartz, which was parallel to the holder. After the growth completion, the vacuum in the chamber was kept at 2×10^{-2} Torr until the temperature slowly dropped to room temperature. Then, the sample was removed from the chamber.

2.3. Analysis of the Samples

The properties of the samples that were ultrasonically cleaned in acetone for a certain period of time (in the same way as the lift-off process), and of those that were not were compared, and the structural, chemical, and electrical characteristics were confirmed. The samples that were ultrasonically cleaned were naturally dried at room temperature and in the absence of sunlight. The surface characteristics of the samples that were prepared using FESEM (HITACHI, S-4800) at a 10–15 kV accelerating voltage and an 8.3–15 mm distance were investigated. The structural characteristics were determined using Raman spectroscopy (NOST, FEX; excitation wavelength: ~ 531 nm; excitation power: ~ 0.3 , ~ 2.9 mW). The chemical components of the samples were analyzed via EDS, and chemical binding was confirmed via XPS (ThermoFisher Scientific, K-Alpha+). In addition, the chemical properties of the dissociated CNW/TiN, whose surface and structural properties were clearly changed by ultrasonic cleaning, were observed. After the samples were submerged in acetone and ultrasonically cleaned for a certain period of time, their electrical charge was examined using Hall measurement (ECOPIA, HMS-3000).

3. Results and Discussion

3.1. Structural Characteristics

The CNWs that were directly grown on Si wafers were dissociated immediately after sonication in acetone. Figure 2a shows the FESEM images of the surface and cross-section of the CNW that was grown directly on a Si wafer. From the cross-section, the height of the CNW was about 800 nm. In addition, the minor particles that were visible on the surface were from the platinum (Pt) coating that was done to achieve a high resolution prior to FESEM shooting. Among the other samples, only those shown in Figure 2b were Pt-coated because a high resolution can be obtained without Pt coating. Figure 2b shows an image of the dissociated CNW/Si wafer, where only the Si wafer can be seen. In Figure 2c, both the CNW grown on the ITO and the catalyst islands (height: about 3 μm) can be seen. The heights of the CNWs grown on the catalyst islands (about 850 nm) and of the CNWs in other parts (about 1 μm) differed from each other by more than about 100 nm. Figure 2d shows the CNW/ITO after ultrasonic cleaning in acetone for 10 min and reveals that compared with its image shown in Figure 2c, there was no change on the surface and in height. Figure 2e shows the growth of the CNWs over TiN; the distance between the walls was narrower than that between the CNWs directly grown on Si wafers shown in Figure 2a. Moreover, the height of the CNW grown on TiN (layer thickness: 150 nm) was about 1.15 μm , about 100 nm higher than that of the CNW grown on ITO. Figure 2f shows the CNW grown on TiN, which was submerged in acetone and ultrasonically cleaned for 5 min. In Figure 2f, partial dissociation can be observed. The right part of this figure is an enlarged image of the dissociated and excavated part of the CNW, and the rest of the lower-height CNW was confirmed.

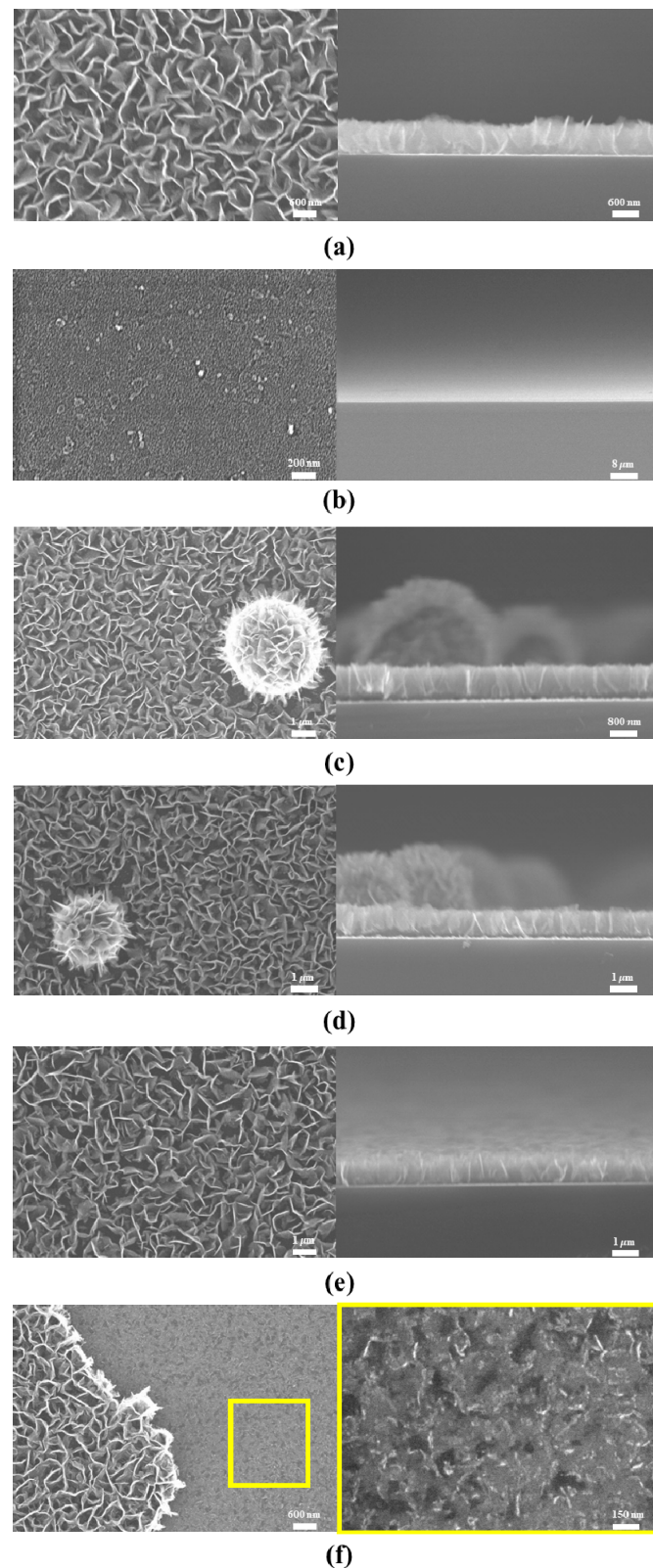


Figure 2. FESEM surface (left) and cross-section (right) images of the carbon nanowall (CNW) directly grown on an Si wafer (a) before and (b) after ultrasonic cleaning in acetone; the CNW grown on ITO (c) before and (d) after ultrasonic cleaning in acetone; and the CNW grown on TiN (e) before and (f) after ultrasonic cleaning in acetone.

The Raman spectrum showed the thickness and defects of graphene through the D and D' peaks ($1350\text{--}1380\text{ cm}^{-1}$), indicating the defect and edge of the graphite nanomaterial; the G peak ($1580\text{--}1600\text{ cm}^{-1}$), indicating the sp^2 structure; and the 2D peak (around 2680 cm^{-1}), indicating the double resonance of the pie bond [24]. In Figure 3a, the structural characteristics are shown by the Raman spectrum of the CNW along the substrate. The Raman spectra of the as-grown CNW and CNW/TiN are similar, but the peaks of CNW/ITO are different; especially, the D and D' peaks are lower than the other peaks. The peaks of D and D' are shown by the same phenomenon, and it can be inferred that the defects and edges of graphene sheets are reduced due to the stable growth of the CNW. Stable growth also causes an increase in adhesion. Figure 3b, on the other hand, shows the Raman spectrum of the CNW/TiN structure when it was submerged in acetone and ultrasonically cleaned for five minutes. When these are compared with Figure 2f, it will be seen that this was the graphite nanomaterial that was dissociated and that remained. In addition, the dissociation from the CNW/TiN structure was very similar to the graphene oxide peak [25]. Figure 3c shows the I_D/I_G ratio, which is the intensity of the D peak divided by that of the G peak, and the I_{2D}/I_G value, which is the intensity of the 2D peak divided by that of the G peak, to identify the defect and thickness of each sample [26,27]. The CNW's I_D/I_G ratio was greater than 1. It can be seen, however, that the G peak, which increased in proportion to the thickness of the graphene layer of CNW/ITO, was larger than the D peak of the defects. This ratio is similar to the I_D/I_G ratio of CNTs [28]. All the samples are multi-layer graphene because the I_{2D}/I_G ratio of the graphene layer thickness indicates a monolayer when it is larger than 2, a few layers when it is larger than 1 and smaller than 2, and a multi-layer when it is smaller than 1.

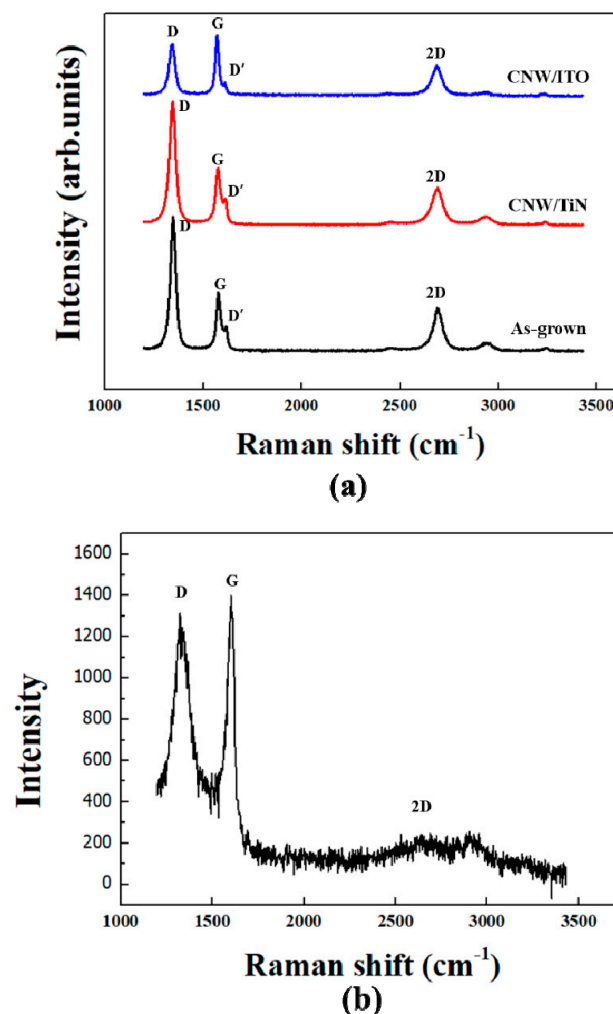


Figure 3. Cont.

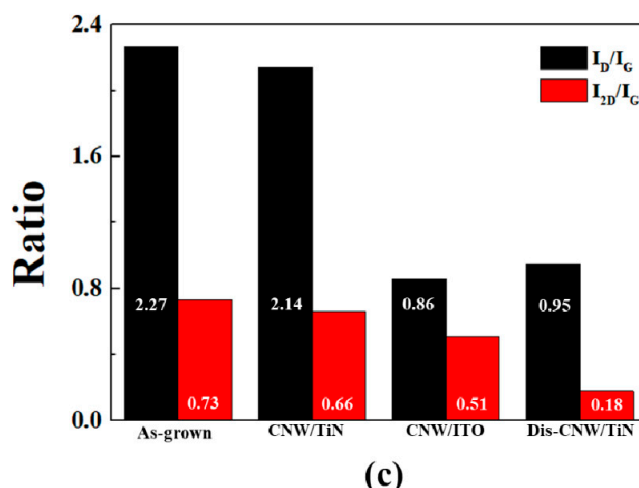


Figure 3. Raman spectra of the (a) as-grown, CNW/ITO, CNW/TiN, and (b) dissociated CNW/TiN, and of the (c) I_D/I_G and I_{2D}/I_G ratios of the samples.

3.2. Chemical Properties

Figure 4a shows the XPS survey and C1s results of the CNW directly grown on a Si wafer. In the survey results, the C1s, O1s, and Si2p peaks can be seen. The O1s peak here appears to have been attached to the CNW due to its exposure to air. Indeed, if the stickiness was caused by the activity of the functional group, the shoulder peak should have been released [29,30], but no significant change in the C1s peak was observed. The peaks of the sp^3 and sp^2 structures were confirmed by the CNW mechanism. When a CNW grows on a substrate, it first forms a buffer layer (or a few graphene layers) and then partially develops defects, causing graphene to grow vertically [6–8,14,31]. Therefore, it becomes a lamellar structure, and when analyzed via XPS, which receives and analyzes the energy at 1–10 nm from the surface, the energy from the flat part (graphene layer) between the walls can be seen on the substrate where the CNW was grown [31]. As such, Figure 4b, which presents the XPS survey results and the C1s peak of CNW/ITO without surface and structural variation even after ultrasonic cleaning, shows the CNW sample grown on ITO, with some In3d and Sn3d peaks. Compared with Figure 4a, the C1s peak decreased, and the O1s peak increased. C1s in the CNW/ITO structure showed some bonds between the oxygen atoms. This was due to the combination of the CNW and the oxygen atoms of ITO, as well as exposure to air. Figure 4c shows the XPS survey results and the C1s peak of CNW/TiN, with the C1s similar to that of the as-grown CNW in Figure 4a. In the survey results, the Ti2p and N1s peaks can be seen, with the same reason for the release of the In3d and Sn3d peaks of CNW/ITO. In Figure 4d, which presents the XPS survey results and the C1s peak of the dissociated CNW/TiN (dis-CNW/TiN), the Ti-C peak after ultrasonic cleaning can be seen, until the CNW had a completely dis-CNW/TiN structure. In the XPS survey, the O1s peak was observed more than the C1s peak, and the Ti2p and N1s peaks increased (compared to the CNW/TiN structure in Figure 4c). The Si2p peak was also observed. Although the peak of the sp^2 structure was higher than that of the sp^3 structure, the peak of the sp^3 structure increased compared to that of the as-grown sample (Figure 4a). The C=O bonding in acetone also increased, indicating that acetone was adsorbed on the CNW.

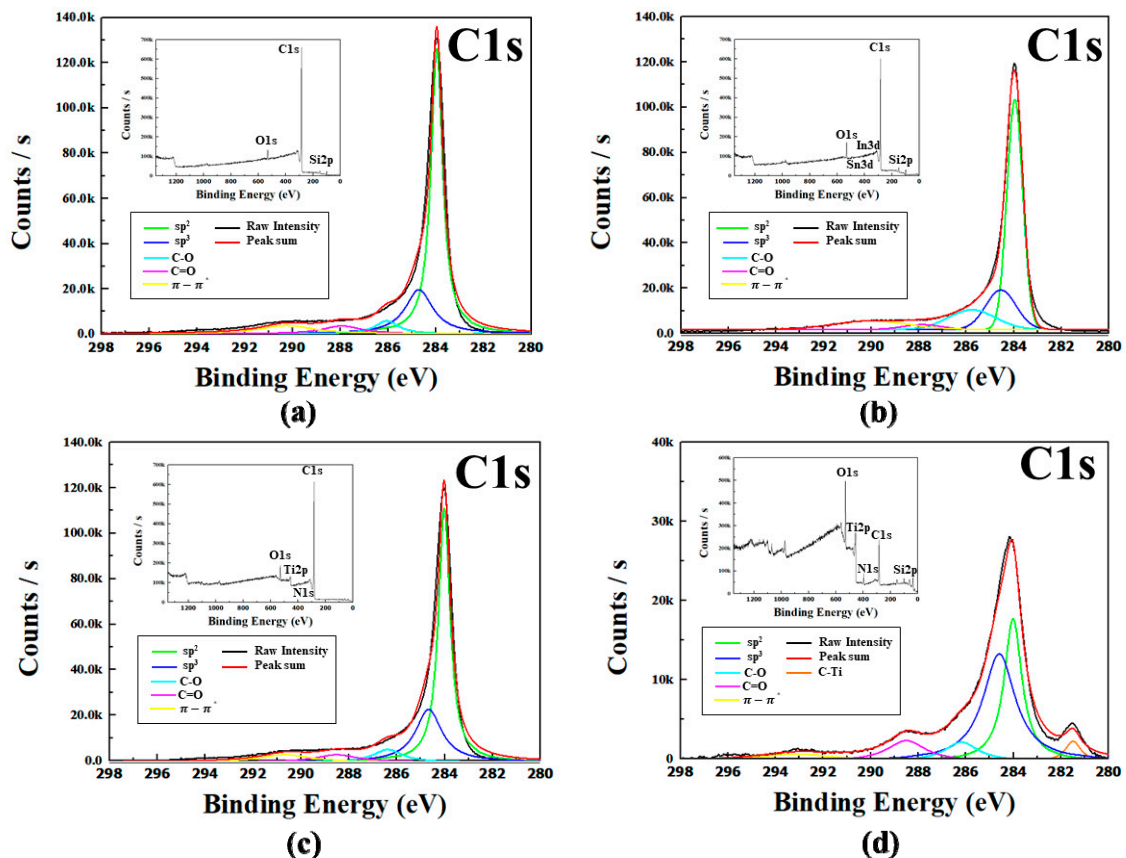


Figure 4. XPS survey results and C1s spectra of the (a) as-grown CNW, (b) CNW/ITO, (c) CNW/TiN, and (d) dissociated CNW/TiN.

Figure 5a shows the Si2p region of CNW/ITO, and it can be seen in the figure that the chemical bond of the Si2p peak in CNW/ITO was Si-C. In addition, the Si2p peak can be more clearly seen than the CNW grown on TiN in Figure 4c. The CNW's bonding to the Si wafer indicates that it was bonded to C, which drilled ITO, and to the Si atoms during the CNW growth via MPECVD. Therefore, ITO becomes a metal with a rough surface (in which the oxygen atoms are carried away, and only indium and tin remain), thereby increasing adhesion [32]. From the O1s peak of dis-CNW/TiN in Figure 5b, the carbonyl group (=O) was found to be larger than the other functional group, and metal carbonate was also observed due to the combination of Ti, C, and O atoms. Figure 5c, which is the Ti2p peak of dis-CNW/TiN, shows Ti atoms combining with O and N atoms. This means that the position of the dissociated carbon was dug, and that it bonded with O atoms. Therefore, it can be said that when the CNW/TiN structure is submerged in acetone and subjected to ultrasonic cleaning, the CNW is dissociated, and ketone attaches to the multi-graphene layer formed by the CNW mechanism, resulting in the formation of graphene oxide with a selectively carbonyl group.

Table 1 shows the FESEM images confirming the chemical components via EDS analysis. All the measurements were examined using 10 K magnification, a 15 mm diameter, and a 15 kV accelerating voltage. In the EDS analysis of the catalyst island in Figure 2c, ITO and CNW components were detected. Furthermore, as the Si atoms were smaller than the other chemical components, the catalyst islands can be inferred from the combination of carbon and ITO. In the other parts of the catalyst islands, however, only small amounts of ITO components were detected. When ITO is hydrogen-plasma-treated at a certain (or higher) temperature, In_2O_3 , a component of ITO, is reduced, and the crystals are destroyed [33,34]. In CNW growth, the $\text{H}_2\text{-CH}_4$ mixture plasma is used, and the growth is made to proceed at a high temperature, so the ITO becomes partially destroyed. Figure 4a,b therefore shows why the Si2p and Si-C peaks were observed. No (or a negligible amount of) O atoms were detected in

the CNW/TiN structure, but CNW/TiN, which was submerged in acetone and ultrasonically cleaned, produced a relatively large amount of O atoms. O atoms were not detected before the ultrasonic cleaning in acetone, but they were subsequently detected, indicating that they were attached to the dissociated CNW/TiN structure.

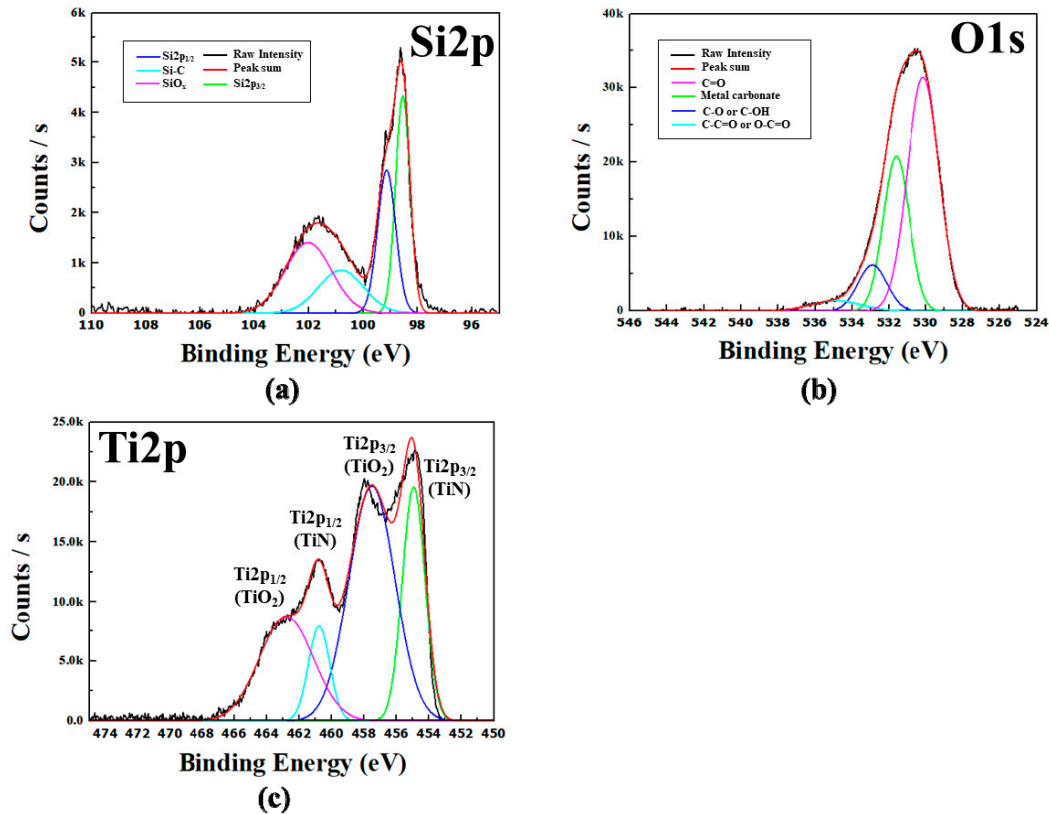


Figure 5. XPS Si2p peak of (a) CNW/ITO, and (b) O1s and (c) Ti2p peaks of the dissociated CNW/TiN.

Table 1. Chemical components of the samples determined via EDS analysis (atomic %).

Samples	C	N	O	Si	In	Sn	Ti
Catalyst island of CNW/ITO	56.71	-	8.24	9.23	17.81	8.02	-
Other parts of CNW/ITO	53.69	-	0.74	45.38	0.03	0.16	-
CNW/TiN	74.44	2.94	-	22.03	-	-	0.57
Dissociated CNW/TiN	16.69	1.50	8.00	72.37	-	-	1.44

3.3. Electrical Characteristics

Hall measurement supplying 1 mA current to the samples was conducted to determine the electrical characteristics of each sample at different ultrasonic cleaning times (0, 1, 10, 20, 30, 50, and 90 min). For greater accuracy, a total of five measurements were made to come up with an average value. The non-changing electrical properties can be inferred from the increased adhesion between the CNW and the substrate under the influence of the interlayer. The CNW that was grown directly on a Si wafer was dissociated immediately after the ultrasonic cleaning, leaving only the Si wafer, which could not be measured by supplying a 1 mA current. When the CNW was grown on the Si wafer, the resistivity was about $1.2 \times 10^{-2} \Omega \cdot \text{cm}$ by Hall measurement. Therefore, the electrical properties of the grown CNW on the interlayer were increased (CNW/ITO: $4.95 \times 10^{-3} \Omega \cdot \text{cm}$; CNW/TiN: $7.43 \times 10^{-3} \Omega \cdot \text{cm}$). Furthermore, the performance of the battery for ESS can be improved by reducing the resistivity, which affects the efficiency [35]. Figure 6a shows the electrical characteristics of the CNW

that was grown on ITO after its ultrasonic cleaning in acetone. When only ITO was deposited on the Si wafer, the carrier concentration was $2.741 \times 10^{20} \text{ cm}^{-3}$, and the resistivity was $1.734 \times 10^{-2} \Omega\cdot\text{cm}$. When CNW was grown on ITO, the electrical characteristics were improved even if ITO was etched with H_2 plasma. Even when ultrasonic cleaning was done for 90 min, the electrical characteristics did not significantly change in the CNW/ITO structure. In addition, the FESEM images obtained after ultrasonic cleaning were the same as those in Figure 2d. Figure 6b shows the electrical characteristics of TiN when it was used as an interlayer. In the case where TiN was deposited on a Si wafer, the electrical characteristics could not be analyzed, only those of the Si wafer. The electrical characteristics were measured, however, after CNW was grown on TiN. TiN has a lower relative dielectric constant than ITO because ITO undergoes spontaneous polarization due to TiN doping, and it can be inferred that ITO has greater adhesive force [36]. The CNW began to dissociate from the moment of its sonication in acetone, was partially dissociated after 1-min ultrasonic cleaning, and was completely dissociated after 10-min ultrasonic cleaning. The area that grew to the size of the $5 \times 5 \text{ mm}^2$ mask was darkened, however, and the FESEM result was as shown in Figure 2f. In addition, even after a 90-min ultrasonic cleaning, the electrical characteristics were shown, and after the complete dissociation following 10-min ultrasonic cleaning, the electrical characteristics of all the samples were in a similar range. From the complete dissociation after 10-min ultrasonic cleaning, the TiN and graphene oxide layers were not easily decomposed by 90-min ultrasonic cleaning due to their strong bonding.

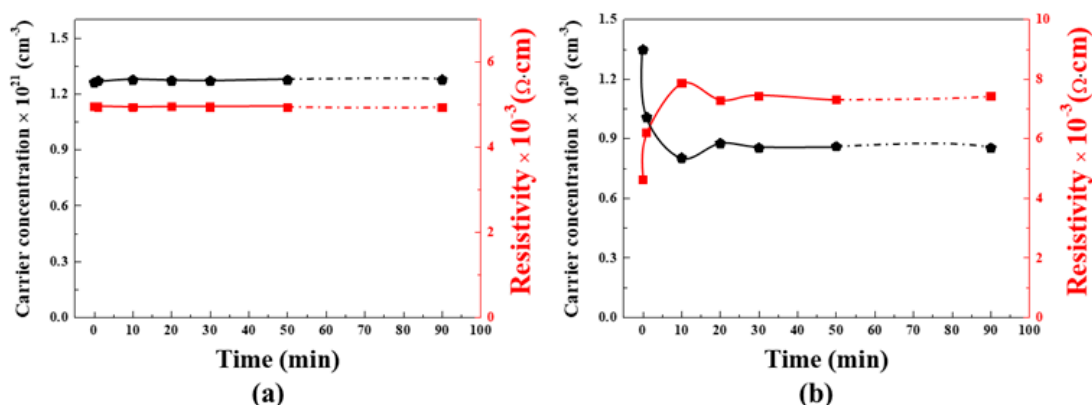


Figure 6. Electrical characteristics of (a) CNW/ITO and (b) CNW/TiN after ultrasonic cleaning in acetone for a certain period of time, obtained via Hall measurement.

4. Conclusions

In this study, to improve the adhesion and electrical properties of carbon nanowalls (CNWs), which are used as the secondary electrode of batteries for energy storage systems (ESSs), CNWs were grown on deposited metal oxide and nitride. An interlayer (indium tin oxide [ITO], titanium nitride [TiN]) was deposited between a CNW and a substrate (Si wafer) to increase their adhesion to each other; the adhesion would be weak if a CNW would be immediately grown on a Si wafer. This is because Si wafers are semiconductors, and ITO and TiN have metal conductivity with better electron sharing or difference in dielectric relative permittivity. Furthermore, ITO loses O atoms and becomes rough due to H_2 plasma during CNW growth on ITO, thereby increasing the adhesion between the CNW and the substrate. The adhesion between the CNW and the substrate was examined after ultrasonic cleaning for a certain period of time following the submergence of the sample in acetone, in the same way as in the lift-off process used in the photolithography process. After the deposition of about 150 nm TiN and ITO on the Si wafer via radio frequency (RF) magnetron sputtering, a CNW was grown via microwave-plasma-enhanced chemical vapor deposition (MPECVD), using a mixture of the methane (CH_4) and hydrogen (H_2) gases. The structural, chemical, and electrical characteristics of the samples were determined before and after ultrasonic cleaning. In the case of CNW/ITO, in which the O atoms of ITO were reduced by H_2 plasma during the CNW growth, the CNW was strongly coupled

with ITO, where the bonding was weakened, and it was not affected by ultrasonic cleaning. In the case of CNW/TiN, the walls were dissociated in a short time by ultrasonic cleaning, but the buffer layer (or graphene layer) formed during the CNW growth remained, combining with the carbonyl group of acetone to produce graphene oxide. After the growth of CNW on ITO, not only the electrical properties increased, but the adhesion increased as well. Thus, CNW/ITO can be utilized for the electrode of secondary batteries through the use of various processes, such as photolithography. On the other hand, it was shown in this study that after the growth of CNW on TiN, the wall is dissociated through ultrasonic cleaning, which reduces the electrical properties, but this may be useful for studies of batteries or other applications using selectively attached functional groups.

Author Contributions: Conceptualization, H.C., S.K.; formal analysis, H.C.; investigation, H.C.; writing—original draft, H.C.; Data curation, S.K.; Writing—review & editing, H.K., J.H.K. and W.C.; Supervision, W.C.

Funding: This work was supported by the Korea Institute of Energy Technology Evaluation and Planning (KETEP) and the Ministry of Trade, Industry, and Energy (MOTIE) of the Republic of Korea (No. 20184030201900), and also by Korea Institute for Advancement of Technology (KIAT) through the Encouragement Program for the Industries of the Economic Cooperation Region (P0002143).

Conflicts of Interest: The authors declare no conflict of interest.

References

1. Sasikala, S.P.; Jeong, G.H.; Yun, T.; Kim, S.O. A perspective on R&D status of energy storage systems in South Korea. *Energy Storage Mater* **2019**, *23*, 154–158. [[CrossRef](#)]
2. Liu, J.; Chen, X.; Yang, H.; Li, Y. Energy storage and management system design optimization for a photovoltaic integrated low-energy building. *Energy* **2019**, *31*, 116424. [[CrossRef](#)]
3. Cheng, L.; Zhang, F.; Liu, S.; Zhang, Z. Configuration method of hybrid energy storage system for high power density in More Electric Aircraft. *J. Power Sources* **2020**, *445*, 227322, in press. [[CrossRef](#)]
4. Zhang, K.; Hu, Z.; Chen, J. Functional porous carbon-based composite electrode materials for lithium secondary batteries. *J. Energy Chem.* **2013**, *22*, 214–225. [[CrossRef](#)]
5. Yang, Q.; Li, J.W.S.; Zhang, L.; Fu, J.; Huang, F.; Cheng, Q. Vertically-oriented graphene nanowalls: Growth and application in Li-ion batteries. *Diam. Relat. Mater.* **2019**, *91*, 54–63. [[CrossRef](#)]
6. Zhu, M.; Wang, J.; Holloway, B.C.; Outlaw, R.A.; Zhao, X.; Hou, K.; Shutthanan, V.; Manos, D.M. A mechanism for carbon nanosheet formation. *Carbon* **2007**, *45*, 2229–2234. [[CrossRef](#)]
7. Zhao, J.; Shaygan, M.; Eckert, J.; Meyyappan, M.; Rummeli, M.H. A Growth Mechanism for Free-Standing Vertical Graphene. *Nano Lett.* **2014**, *14*, 3064–3071. [[CrossRef](#)]
8. Bo, Z.; Yang, Y.; Chen, J.; Yu, K.; Yan, J.; Cen, K. Plasam-enhanced chemical vapor deposition synthesis of vertically oriented graphene nanosheets. *Nanoscale* **2013**, *5*, 5180. [[CrossRef](#)]
9. Kumar, A.; Voevodin, A.A.; Zemlyanov, D.; Zakharov, D.N.; Fisher, T.S. Rapid synthesis of few-layer graphene over Cu foil. *Carbon* **2012**, *50*, 1546–1553. [[CrossRef](#)]
10. Zhang, J.; Tahmasebi, A.; Omoriyekomwan, J.E.; Yu, J. Production of carbon nanotubes on bio-char at low temperature via microwave-assisted CVD using Ni catalyst. *Diam. Relat. Mater.* **2019**, *91*, 98–106. [[CrossRef](#)]
11. Cui, L.; Chen, J.; Yang, B.; Sun, D.; Jiao, T. RF-PECVD synthesis of carbon nanowalls and their field emission properties. *Appl. Surf. Sci.* **2015**, *357*, 1–7. [[CrossRef](#)]
12. Banerjee, D.; Mukherjee, S.; Chattopadhyay, K.K. Synthesis of amorphous carbon nanowalls by DC-PECVD on different substrates and study of its field emission properties. *Appl. Surf. Sci.* **2011**, *257*, 3717–3722. [[CrossRef](#)]
13. Obraztsov, A.N.; Volkov, A.P.; Nagovitsyn, K.S.; Nishimura, K.; Morisawa, K.; Nakano, Y.; Hiraki, A. CVD growth and field emission properties of nanostructured carbon films. *J. Phys. D Appl. Phys.* **2002**, *35*, 357–362. [[CrossRef](#)]
14. Kim, S.Y.; Shin, S.K.; Kim, H.; Jung, Y.H.; Kang, H.; Choi, W.S.; Kweon, G.B. Synthesis of Carbon Nanowalls by Microwave PECVD for Battery Electrode. *Trans. Electr. Electron. Mater.* **2015**, *16*, 198–200. [[CrossRef](#)]
15. Obraztsov, A.N.; Pavlovsky, I.Y.; Volkov, A.P.; Petrov, A.S.; Petrov, V.I.; Rakova, E.V.; Roddatis, V.V. Electron field emission and structural properties of carbon chemically vapor-deposited films. *Diam. Relat. Mater.* **1999**, *8*, 814–819. [[CrossRef](#)]

16. Lee, S.W.; Muoth, M.; Helbling, T.; Mattmann, M.; Hierold, C. Suppression of resist contamination during photolithography on carbon nanomaterials by a sacrificial layer. *Carbon* **2014**, *66*, 295–301. [[CrossRef](#)]
17. Filippidou, M.K.; Chatzichristidi, M.; Chatzandroulis, S. A fabrication process of flexible IDE capacitive chemical sensors using a two step lift-off method based on PVA patterning. *Sens. Actuators B Chem.* **2019**, *284*, 7–12. [[CrossRef](#)]
18. Aleksandrova, M.; Kurtev, N.; Videkov, V.; Tzanova, S.; Schintke, S. Material alternative to ITO for transparent conductive electrode in flexible display and photovoltaic devices. *Microelectron. Eng.* **2015**, *145*, 112–116. [[CrossRef](#)]
19. Li, Z.H.; Cho, E.S.; Kwon, S.J. Laser direct patterning of the T-shaped ITO electrode for high-efficiency alternative current plasma display panels. *Appl. Surf. Sci.* **2010**, *257*, 776–780. [[CrossRef](#)]
20. Virolainen, S.; Huhtanen, T.; Laitinen, A.; Sainio, T. Two alternative process routes for recovering pure indium from waste liquid crystal display panels. *J. Clean. Prod.* **2020**, *243*, 118599, in press. [[CrossRef](#)]
21. Aal, A.A. Development of nickel coatings by TiN interlayer. *Mater. Chem. Phys.* **2007**, *106*, 317–322. [[CrossRef](#)]
22. Zhou, B.; Liu, Z.; Piliptsov, D.G.; Rogachev, A.V.; Yu, S.; Wu, Y.; Tang, B.; Rudenkov, A.S. Growth feature of ionic nitrogen doped CN_x bilayer films with Ti and TiN interlayer by pulse cathode arc discharge. *Appl. Surf. Sci.* **2016**, *361*, 169–176. [[CrossRef](#)]
23. Kern, W.; Puotinen, D.A. Cleaning solutions based on hydrogen peroxide for use in silicon semiconductor technology. *RCA Rev.* **1970**, *31*, 187.
24. Malard, L.M.; Pimenta, M.A.; Dresselhaus, G.; Dresselhaus, M.S. Raman spectroscopy in graphene. *Phys. Rep.* **2009**, *473*, 51–87. [[CrossRef](#)]
25. Pérez, L.A.; Bajales, N.; Lacconi, G.I. Raman spectroscopy coupled with AFM scan head: A versatile combination for tailoring graphene oxide/reduced graphene oxide hybrid materials. *Appl. Surf. Sci.* **2019**, *495*, 143539. [[CrossRef](#)]
26. Graf, D.; Molitor, F.; Ensslin, K.; Stampfer, C.; Jungen, A.; Hierold, C.; Witz, L. Spatially resolved Raman spectroscopy of single- and few-layer graphene. *Nano Lett.* **2007**, *7*, 238–242. [[CrossRef](#)]
27. Ferrari, A.C.; Meyer, J.C.; Scardaci, V.; Casiraghi, C.; Lazzeri, M.; Mauri, F.; Piscanec, S.; Jiang, D.; Novoselov, K.S.; Roth, S.; et al. Raman spectrum of graphene and graphene layers. *Phys. Rev. Lett.* **2006**, *97*, 187401–187404. [[CrossRef](#)]
28. Soin, N.; Roy, S.S.; Ray, S.C.; McLaughlin, J.A. Excitation energy dependence of Raman bands in multiwalled carbon nanotubes. *J. Raman Spectrosc.* **2010**, *41*, 1227–1233. [[CrossRef](#)]
29. Al-Gaashani, R.; Najjar, A.; Zakaria, Y.; Mansour, S.; Atieha, M.A. XPS and structural studies of high quality graphene oxide and reduced graphene oxide prepared by different chemical oxidation methods. *Ceram. Int.* **2019**, *45*, 14439–14448. [[CrossRef](#)]
30. Ederer, J.; Janoš, P.; Ecorchard, P.; Tolasz, J.; Štengl, V.; Beneš, H.; Perchacz, M.; Pop-Georgievski, O. Determination of amino groups on functionalized graphene oxide for polyurethane nanomaterials: XPS quantitation vs. functional speciation. *RSC Adv.* **2017**, *21*, 12464–12473. [[CrossRef](#)]
31. Zhang, L.X.; Sun, Z.; Qi, J.L.; Shi, J.M.; Hao, T.D.; Feng, J.C. Understanding the growth mechanism of vertically aligned graphene and control of its wettability. *Carbon* **2016**, *103*, 339–345. [[CrossRef](#)]
32. Vitos, L.; Ruban, A.V.; Skriver, H.L.; Kollár, J. The surface energy of metals. *Surf. Sci.* **1998**, *411*, 186–202. [[CrossRef](#)]
33. Lim, W.; Ahn, Y.; Lee, S.; An, I.; Lee, C. The stability of ITO, AZO and SZO thin films in hydrogen plasma. *J. Korean Vac. Soc.* **1997**, *6*, 227–234.
34. Lee, J.; Lim, D.; Yang, K.; Choi, W. Influence of different plasma treatments on electrical and optical properties on sputtered AZO and ITO films. *J. Cryst. Growth.* **2011**, *326*, 50–57. [[CrossRef](#)]
35. Yue, Z.; Zhou, L.; Jin, C.; Liu, L.; Xu, G.; Tang, H.; Huang, H.; Yuan, J.; Gao, C. Study on the effect of intrinsic electrical resistivity of silicon materials on its performance for Li-ion batteries. *Mater. Lett.* **2017**, *186*, 217–219. [[CrossRef](#)]
36. Akherat, S.J.M.; Karimi, M.A.; Alizadehyazdi, V.; Asalzadeh, S.; Spenko, M. A tunable dielectric to improve electrostatic adhesion in electrostatic/microstructured adhesives. *J. Electrostat.* **2019**, *97*, 58–70. [[CrossRef](#)]

